Development of Compton X-Ray Spectrometer
for Fast Ignition Experiment[*]

Sadaoki KOJIMA, Yasunobu ARIKAWA, Takahito IKENOUCHI, Takahiro NAGAI, Yuki ABE,
Shouhei SAKATA, Hiroaki INOUE, Takuya NAMIMOTO, Shinsuke FUJIOKA, Mitsuo NAKAI,
Hiroyuki SHIRAGA, GEKKO-XII&LFEX Team, Tetsuo OZAKI[1], Makoto R. ASAKAWA[2],
Ryukou KATO[3] and Hiroshi AZECHI

Institute of Laser Engineering, Osaka University, 2-6 Yamada-oka, Suita 565–0871, Japan
[1]*National Institute for Fusion Science, 322-6 Oroshi-cho, Toki 509-5292, Japan*
[2]*Faculty of Engineering Science, Kansai University, 3-3 Yamate, Suita 564-8680, Japan*
[3]*Institute of Scientific and Industrial Research, Osaka University, 2-6 Yamada-oka, Suita 565-0871, Japan*

In the context of Fast Ignition, the fast electron temperature is a key parameter to determine the laser-to-fast electron energy conversion efficiency. Bremsstrahlung X-ray (γ-ray) emission represents an attractive alternative to measure this fundamental parameter. In this study, a single-shot high-energy γ-ray spectrometer with sensitivity ranging from 0.5 MeV to 7 MeV was developed, allowing to estimate the γ-ray spectrum in the fast ignition.

1. Inroduction

Fast Ignition (FI) is an alternative approach to Inertial Confinement Fusion, consisting in the separation of the compression and heating stages. In FI, the heating of the compressed Deuterium-Tritium (DT) fuel is produced by a ultra-high intensity laser-generated fast electron beam depositing its energy in the high density plasma by Coulomb interaction. The coupling efficiency is strongly dependent on the fast electron energy distribution, therefore representing a crucial parameter to be diagnosed [1]. From simulations, in order to ignite a compressed DT pellet having density of 300 g/cm^3, 18 kJ of fast electron energy has to be deposited within a diameter of 40 μm in the compressed fuel. Fast electrons in the 1-3 MeV energy range are responsible for the energy deposition in such a small volume, allowing for the creation of a lateral hot spot. Thus high conversion efficiency into 1-3 MeV energy range fast electrons is fundamental for the achievement of Fast Ignition [2–4]. However, it is difficult to measure initial fast electron temperature from the outside of plasma because of the strong sheath potential around the target. The bremsstrahlung X-ray is an attractive alternative diagnostic for this aim. In previous works, many kind of γ-ray detectors with different sensitivities have been developed. Various techniques have been adopted to measure the fast electron energy spectrum, such as vacuum electron spectroscopy, nuclear activation, Bremsstrahlung, buried fluorescent foils, proton emission, and coherent transition radiation [5–9]. Filter stack technique uses differential filtering to discriminate the γ-ray spectrum [10, 11]. The spectrometer consists of thirteen filters of increasing Z, five 100 μm thick filters Al, Ti, Fe, Cu and Mo, followed by 150 μm Ag, 500 μm Sn and Ta filters, and one 1.58 mm Au filter. Finally four Pb filters with thickness varying from 1 mm to 4 mm for differential filtering are positioned in the stack. Nuclear activation technique uses photo nuclear activation to discriminate the γ-ray spectrum. In this method, γ-ray spectrum is measured from the activation ratio of a pseudo-alloy consisting of gold (^{197}Au), tantalum (^{181}Ta), niobium (^{93}Nb), and chromium (^{50}Cr, ^{52}Cr, ^{53}Cr, ^{54}Cr) with mass fraction being 43.25%, 24.25%, 16.25%, 16.25%, respectively [12]. However, observable energy range of these two detectors are respectively up to 0.5 keV and above 7 MeV, respectively. Thus, these materials are unsuitable to measure γ-ray s in the range 1-3 MeV which represents the energy range of our interest. In this study, a single-shot high-energy γ-ray spectrometer, with sensitivity from 0.5 keV to 7 MeV, was developed, allowing for the first time to estimate of the fast electron-generated bremmstrahlung X-ray spectrum.

2. Diagnostic Design
2.1 Measurement of X-ray energy

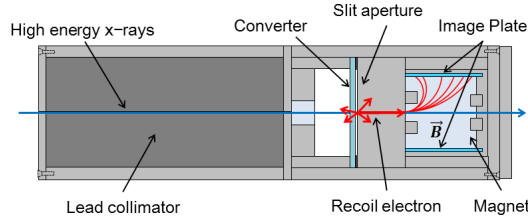Photons with energy around 1 MeV mainly interact with matter by Compton scattering, the energy of incident

Fig. 1 The structure of developed detector. The structure of the Compton X-ray spectrometer consists of a lead collimator, converter and an electron spectrometer.

X-rays can be measured by measuring the energy and the angle of recoil electrons. The structure of the Compton X-ray spectrometer is shown in Fig. 1. The high energy X-rays emitted from the target are initially collimated by means of a lead collimator. Then, the collimated X-rays recoil electrons via Compton scattering in the converter. The energy of the electrons crossing the aluminum slit set in front of the converter is measured by means of an electron spectrometer (ESM) and the data recorded on Image Plate (IP).

2.2 Converter

The material composing the converter is chosen in order to have high conversion efficiency from X-rays to recoiled electrons and low energy absorption in the converter. The material is selected by estimating these two parameters from X-ray-matter interaction cross sections, electron stopping power and Coulomb scattering.

Cross sections of each factor can be approximated as

$$\sigma_{\text{compton}} \propto NZ(h\nu)^{-1} \tag{1}$$

$$\sigma_{\text{photo}} \propto NZ^5(h\nu)^{-\frac{7}{2}} \tag{2}$$

$$\sigma_{\text{pair}} \propto NZ^2(h\nu - 1.02) \tag{3}$$

$$-\frac{dE}{dx} \propto NZ \tag{4}$$

$$\sigma_{\text{scatter}} \propto \frac{Z^2}{(h\nu)^2} \tag{5}$$

where N is the number of the atom per cm^3, Z is the atomic number and $h\nu$ is the incident photon energy.

Cross sections for Compton scattering and stopping power depend linearly on the atomic number. On the other hand, Cross sections for photoelectric absorption, pair creation and Coulomb scattering have a non-linear dependence on Z.

Figure 2 shows Monte Carlo simulation results of Coulomb scattering in the converter simulated by Casino ver.2.42 [13]. The red lines and the blue lines show respectively the trajectories of back-scattered and forward scattered electrons. In high-Z material, efficiency of the back scattering increase due to strong Coulomb potential around the nuclear.

Figure 3 shows the cross sections for photoelectric effect, Compton scattering and pair production in low and
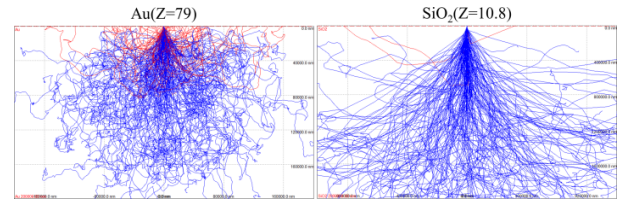

Fig. 2 Trajectory of electrons in the converter simulated by Casino ver.2.42. (a) Gold foil (high Z) and (b) Silica plate (low Z). In high-Z material, efficiency of the back scattering shown by red lines increase due to strong Coulomb potential around the nuclear.
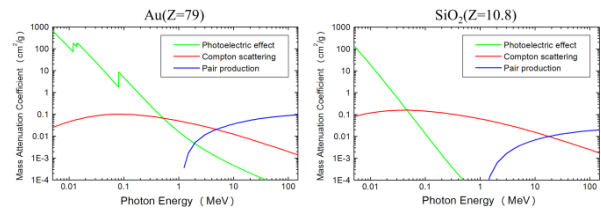

Fig. 3 Cross section for the three interactions. (a) Gold (high Z) and (b) Silica (low Z). Low Z material must be chosen in order to maximize the Compton scattering produced electron.

high Z material, respectively SiO$_2$ and Au. Being the cross section for photoelectric effect proportional to Z to the fifth power, low Z material must be chosen in order to maximize the Compton scattering produced electron.

Following the discussion above, a thick, low Z converter material is the optimal choice. Due to alignment requirements, a transparent material was needed. A BK glass provides at the same time the characteristics of transparency and low Z material.

2.3 Background reduction

A lead box and two magnets were designed to shield respectively X-rays and charged particle produced background on the IP detector. A second IP is positioned in front of the recoil electron IP detector in order to measure positron signal in the unlikely case of pair production in the converter.

3. Calibration Experiments by Using ^{60}Co

Cobalt60 decays in two possible ways, emitting two γ rays which energy is respectively 1.1732 MeV and 1.3325 MeV. The new detector was tested by diffracting γ-rays emitted by ^{60}Co. As converter, a thin 50 μm Au foil was chosen, in order to guarantee low recoil electron energy loss in the converter. Figure 4 represents the recoil electron spectrum from ^{60}Co. Experimental data are represented by red dots, while the Black line represents the Monte Carlo simulation result taking into account the de-
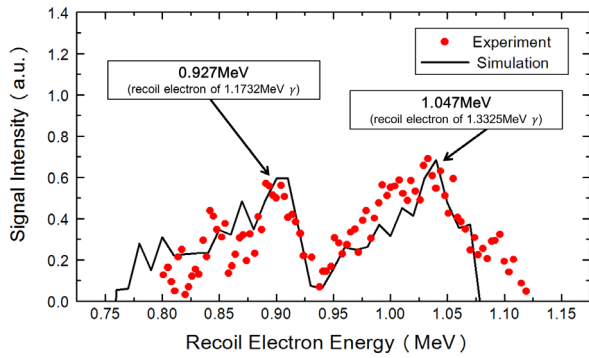
Fig. 4 Recoil electron signal from ^{60}Co. Experimental data are represented by red dots while the Black line represents the Monte Carlo simulation. The energy resolution is obtained via Gaussian fitting of the two peaks, and is estimated to be 10.4% for 1.1732 MeV and 11.2% for 1.3325 MeV respectively.
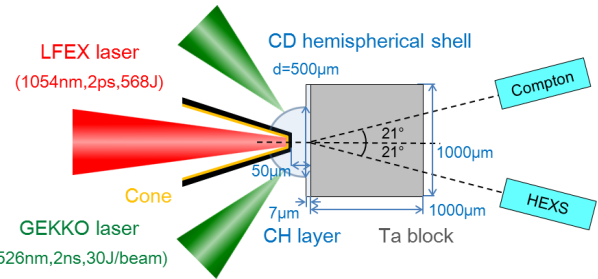

Fig. 5 Experimental setup. The target was constituted by a cone-in-shell, adopting an hemispherical shell configuration. The shell was mounted on a cubic Ta block.
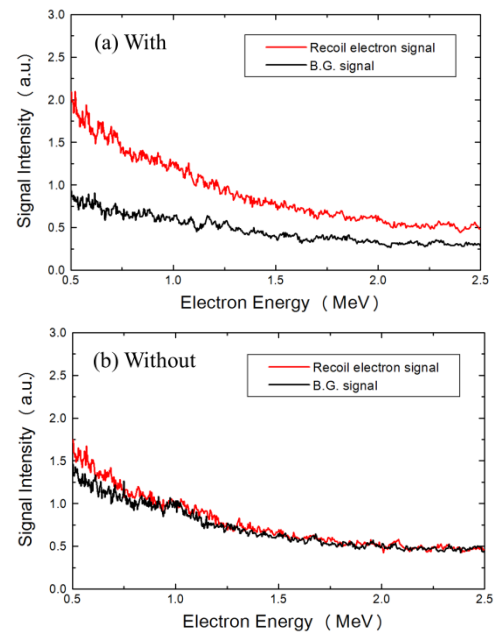

Fig. 6 Signals recorded by the detector. (a) with converter, (b) without converter.

tector energy resolution. In Fig. 4, the experimental result is represented for ^{60}Co gamma-ray detection. The energy resolution is high enough to allow detecting two distinct peaks corresponding to the two γ photon energy. The energy resolution is obtained via Gaussian fitting of the two peaks, and is estimated to be 10.4% for 1.1732 MeV and 11.2% for 1.3325 MeV respectively.

4. Fast Ignition Experiment
4.1 Experimental setup

The experiment was performed at GEKKO laser facility, Institute of Laser Engineering, Osaka University. GEKKO laser delivers up to 12 beams of ~300 J energy arranged in spherical geometry. Coupled to GEKKO laser LFEX, a ultra-high intensity beam capable of deliver ~5 kJ of laser light onto a ~50 µm focal spot in 1-10 ps.

Typical γ-rays were generated by using LFEX&GEKKO laser. The target was constituted by a cone-in-shell, adopting an hemispherical shell configuration, as shown in Fig. 5. The shell was mounted on a cubic Ta block of 1 mm lateral size. The distance from the cone tip to the Ta block was 50 µm. Three frequency doubled (527 nm) GEKKO beams, delivering 30 J each of laser energy, were focused onto the hemispheric CD shell producing a low Z and low density ($n_e \sim 1.4 \times 10^{22}$ cm^{-3}) plasma medium between the cone and the Ta block. Subsequently, 568 J, 1054 nm and 1 ps long LFEX pulse were focused at the cone tip to produce a fast electron beam, propagating through the low density CD plasma into the Ta block. Part of the fast electron energy is converted in γ-rays into the Ta block, which emission is measured by means of the Compton scattering spectrometer (Compton) and a High Energy X-ray Spectrometer (HEXS), the latest set at 21° relatively to the LFEX laser axis.

The HEXS diagnostic is based on the widely used multiple filter stack detector technique. Experimental re-

sults for the Compton spectrometer are reported in Figs. 6, 7. The Compton spectrometer has been operated with and without converter foil during the experiment and results are represented in Fig. 6. The recoil electron signal is represented in red while the background signal in black. From experimental data it appears clear that the background electron signal collected without converter layer is much smaller than the recoil electron signal in presence of converter.

4.2 Analysis method

Recoil electron spectrum can be expressed as the sum of multiple spectral distributions (see Eq. (6)). The spectrum of γ-rays-produced photoelectrons was simulated using the Monte Carlo code MCNP5 [14] using the spectrum in Eq. (6). The free parameters constituted by the 3 amplitudes R1, R2 and R3 and the 3 relative electron temperatures T1, T2 and T3 are obtained by fitting the experimen-
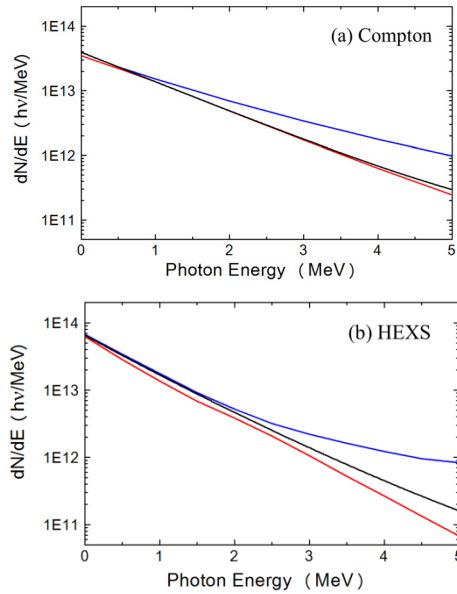
Fig. 7 (a) γ-ray spectrum measured by Compton spectrometer. (b) Filter stack detector. The black solid line show the best fit distribution, red and blue lines represent respectively the lower and the upper limit of our solution.

tal data with the Monte Carlo simulation.

$$f(E) = R_1 \exp\left(-\frac{E}{T_1}\right) + R_2 \exp\left(-\frac{E}{T_2}\right) + R_3 \exp\left(-\frac{E}{T_3}\right)$$

(6)

in the simulation T_1, T_2, T_3 varied from 0.1 MeV to 10 MeV and R_1 and R_2 respectively varied from 1 to 10000 and 1 to 1000 while R_3 is considered to be 1. Figures 7 (a) and (b) show the X-ray spectrum obtained by the filter stack detector (HEXS) and the Compton spectrometer, respectively. In Fig. 7, the black solid line show the best fit distribution, red and blue lines represent respectively the lower and the upper limit of our solution, imposed by the fitting error and detector response error.

We successfully measured γ-ray spectrum in fast ignition related experiment and data from the two diagnostics are in good agreement.

5. Conclusions

In this study, a single-shot, high-energy Compton X-ray spectrometer with the sensitivity up to 7 MeV has been developed. From experimental data, the energy resolution of the detector is estimated to be the 10.4% for 1.1732 MeV γ-rays, and the 11.2% for 1.3325 MeV γ-rays. γ-rays in the energy range from 0.5 to 2.5 MeV have been measured. These correspond to fast electrons which penetration range is optimum for compressed DT plasma heating in a Fast Ignition scenario. By comparison with the HEXS diagnostic, the Compton scattering diagnostic allows for the determination of the γ-ray spectrum and the determination of the absolute photon number per unit energy, allowing, at the same time, for a more accurate determination of the γ-ray energy spectrum compared to HEXS. Indeed for a specific data acquisition with the HEXS, there are multiple γ-ray spectra that can reproduce the same data. The Compton spectrometer data instead are univocally determined. Moreover the energy spectrum recorded by the Compton spectrometer is much larger than that one recorded by the HEXS, allowing to detect γ-rays having energies up to 7 MeV.

[1] R. Kodama, H. Shiraga, K. Shigemori, Y. Toyama, S. Fujioka, H. Azechi, H. Fujita, H. Habara, T. Hall, Y. Izawa, T. Jitsuno, Y. Kitagawa, K.M. Krushelnick, K.L. Lancaster, K. Mima, K. Nagai, M. Nakai, H. Nishimura, T. Norimatsu, P.A. Norreys, S. Sakabe, K.A. Tanaka, A. Youssef, M. Zepf and T. Yamanaka, Nature **418**(6901), 933 (2002).

[2] S. Atzeni, A. Schiavi and C. Bellei, Phys. Plasmas **14**(5), 052702 (2007).

[3] R. Kodama, P.A. Norreys, K. Mima, A.E. Dangor, R.G. Evans, H. Fujita, Y. Kitagawa, K. Krushelnick, T. Miyakoshi, N. Miyanaga, T. Norimatsu, S.J. Rose, T. Shozaki, K. Shigemori, A. Sunahara, M. Tampo, K.A. Tanaka, Y. Toyama, T. Yamanaka and M. Zepf, Nature **412**(6849), 798 (2001).

[4] M. Tabak, J. Hammer, M.E. Glinsky, W.L. Kruer, S.C. Wilks, J. Woodworth, E.M. Campbell, M.D. Perry and R.J. Mason, Phys. Plasmas **1**(5), 1626 (1994).

[5] K.A. Tanaka, R. Kodama, H. Fujita, M. Heya, N. Izumi, Y. Kato, Y. Kitagawa, K. Mima, N. Miyanaga, T. Norimatsu, A. Pukhov, A. Sunahara, K. Takahashi, M. Allen, H. Habara, T. Iwatani, T. Matusita, T. Miyakosi, M. Mori, H. Setoguchi, T. Sonomoto, M. Tanpo, S. Tohyama, H. Azuma, T. Kawasaki, T. Komeno, O. Maekawa, S. Matsuo, T. Shozaki, K. Suzuki, H. Yoshida and T. Yamanaka, Phys. Plasmas **7**(5), 2014 (2000).

[6] T. Iwawaki, H. Habara, T. Tanimoto, N. Nakanii, K. Shimada, T. Yabuuchi, K. Kondo and K.A. Tanaka, Rev. Sci. Instrum. **81**, 10E535 (2010).

[7] S.P. Hatchett, C.G. Brown, T.E. Cowan, E.A. Henry, J.S. Johnson, M.H. Key, J.A. Koch, A.B. Langdon, B.F. Lasinski, R.W. Lee, A.J. Mackinnon, D.M. Pennington, M.D. Perry, T.W. Phillips, M. Roth, T.C. Sangster, M.S.

Singh, R.A. Snavely, M.A. Stoyer, S.C. Wilks and K. Yasuike, Phys. Plasmas **7**, 2076 (2000).

[8] K. Yasuike, M.H. Key, S.P. Hatchett, R.A. Snavely and K.B. Wharton, Rev. Sci. Instrum. **72**(1), 1236 (2001).

[9] W. Theobald, K. Akli, R. Clarke, J.A. Delettrez, R.R. Freeman, S. Glenzer, J. Green, G. Gregori, R. Heathcote, N. Izumi, J.A. King, J.A. Koch, J. Kuba, K. Lancaster, A.J. MacKinnon, M. Key, C. Mileham, J. Myatt, D. Neely, P.A. Norreys, H.-S. Park, J. Pasley, P. Patel, S.P. Regan, H. Sawada, R. Shepherd, R. Snavely, R.B. Stephens, C. Stoeckl, M. Storm, B. Zhang and T. C. Sangster, Phys. Plasmas **13**(4), 043102 (2006).

[10] B. Westover, C.D. Chen, P.K. Patel, M.H. Key, H. McLean, R. Stephens and F.N. Beg, Phys. Plasmas **18**, 063101 (2011).

[11] C.D. Chen, P.K. Patel, D.S. Hey, A.J. Mackinnon, M.H. Key, K.U. Akli, T. Bartal, F.N. Beg, S. Chawla, H. Chen, R.R. Freeman, D.P. Higginson, A. Link, T.Y. Ma, A.G. MacPhee, R.B. Stephens, L.D. Van Woerkom and B. Westover, Phys. Plasmas **16**, 082705 (2009).

[12] M.M. Günther, K. Sonnabend, E. Brambrink, K. Vogt, V. Bangnoud, K. Harres and M. Roth, Phys. Plasmas **18**, 083102 (2011).

[13] D. Drouin, A. Réal Couture, D. Joly, X. Tastet, V. Aimez and R. Gauvin, Scanning **29**, Issue3, 92 (2007).

[14] J.F. Briesmeister (ed) 1988 MCNP - A General Monte Carlo N-Particle Transport Code. Version 4A, LA-12625-M (Los Alomos, NM: Los Alamos National Laboratory).